Int J Adv Manuf Technol (2017) 89:711–725
DOI 10.1007/s00170-016-9140-0

ORIGINAL ARTICLE

Weld quality prediction in friction stir welding using wavelet analysis

Bipul Das[1] · **Sukhomay Pal**[1] · **Swarup Bag**[1]

Received: 29 August 2015 / Accepted: 4 July 2016 / Published online: 8 July 2016
© Springer-Verlag London 2016

Abstract The paper aims to present the application of wavelet packet transformation for feature extraction from the signals acquired during friction stir welding of aluminum alloy. One of the challenges encountered while implementing wavelet packet transformation is the selection of an appropriate mother wavelet function. In this study, a new method is proposed for the selection of an appropriate mother wavelet function based on the ratio of energy of the signal to the entropy of the decomposed wavelet packets. Main spindle motor and feed motor current signals are acquired during 65 welding experiments designed through full factorial method by varying three process parameters in four levels. Features obtained from wavelet packet transformation along with process parameters are fed to two artificial neural network models: multi-layer feed-forward neural network model trained with back propagation algorithm and radial basis function neural network model for the prediction of ultimate tensile strength and yield strength of the welds. The prediction performance of the former model is found to be superior to the later model for both ultimate tensile strength and yield strength.

Keywords Friction stir welding · Weld quality monitoring · Wavelet packet analysis · Neural network modeling · Strength prediction · Mother wavelet selection

✉ Sukhomay Pal
spal@iitg.ernet.in

[1] Department of Mechanical Engineering, Indian Institute of Technology Guwahati, Guwahati, Assam 781039, India

1 Introduction

The scope of recent welding industries is not limited to fabricate conventional commodities using conventional processes as different processes have been evolved for welding of different materials. The process of friction stir welding (FSW) since its invention offered more flexibility to use various difficult-to-weld materials to find its application in different industries such as railways, automation, aviation, etc. In today's automated manufacturing environment, quality of output from every sub-process added towards the final quality index of the product in the production chain and welding is certainly a momentous sub-process in many manufacturing industries. As FSW found its extensive use in different industrial applications, consequently, different methods are in demand for precise prediction of weld quality at different welding conditions.

Direct and indirect techniques are available for weld quality measurement. Direct methods include visual inspection and vision sensing. Indirect techniques involve measurement of some signals to establish correlation with the weld quality. The process of FSW closely resembles to the forming process [1], where different forces play influencing role to govern the process for desired output. Forces associated with FSW process were investigated by Boldsaikhan et al. [2] to correlate with the weld quality. Discrete Fourier transformation was used to analyze the force signals for detection of defects in the weld and to develop a method for monitoring the weld quality. Trummera et al. [3] studied the effect of clamping force on the joint strength in FSW process. Yang et al. [4] and Fleming et al. [5] used force signals for detection of gap in FSW process. The effect of different process parameters in FSW was investigated through force signals by Cavaliere et al. [6]. Trimble et al. [7] studied the effect of different pin profiles in the process outcome in FSW process by measuring

force signals during the process. A combined wavelet packet and Hilbert-Huang transform was proposed by Das et al. [8] for monitoring of FSW process using real-time force signals. Defect assessment along with weld strength modeling was achieved, and it was concluded that the proposed approach was effective in FSW process.

Apart from force signals, acoustic emission signals are also found important in monitoring of FSW process. Subramaniam et al. [9] investigated the effect of tool pin profile on joint strength in FSW process through acoustic emission signal analysis. Discrete Fourier transformation was used as a signal processing tool for analyzing the acoustic emission signals. Wavelet transformation was used as a signal processing tool by Chen et al. [10] for the monitoring of FSW process. Acoustic emission signals were recorded during experiment and a methodology for detection of gap was proposed. Zeng et al. [11] correlated the information contained in acoustic emission signal to the tool wear in FSW process and investigated the effect of it on the weld quality.

The aforementioned survey of available research work conveyed the message that force signals were mostly used in monitoring of FSW process which is followed by acoustic emission signals. In general, force is considered as one of the most significant variables in the FSW process. But, the limitation with this method is the cost associated with the system for acquiring force signals. Apart from this, the signals are often found to be corrupted with noise [4] which needs to be filtered before presenting to the monitoring algorithm. In case of acoustic emission signals also, chances of the signal getting corrupted with noise pursued. In other manufacturing processes, researchers have reported to use other signals such as current and voltage for monitoring of the process. Pal et al. [12] captured the current and voltage signatures of the arc during pulsed metal inert gas welding and correlated the information to predict the weld quality. An extensive review work by Sick [13] stated the research efforts in the field of turning operation where different signals were measured and analyzed for the prediction of tool wear, built-up edge formation, and surface condition of the workpiece during turning. Tool wear measurement and classification using artificial intelligence in boring operation were presented by Liu et al. [14] using the features extracted from cutting force signals.

It has been proven that current sensor is an effective sensor for monitoring of other welding and manufacturing processes [12, 15–18]. It is also inexpensive compared to force and acoustic emission sensors. The chances of getting noisy signal are less, and it can be used without altering an existing setup/machine. Das et al. [19] reported that current signals can be effectively implemented in monitoring of FSW process. Current signals are analyzed in time domain, and root mean square values of signals were computed to develop regression models to correlate with weld quality. In FSW process, the joint strength is the combined effect of tool rotational speed and welding speed. Therefore, current signals of both spindle and feed motors can be used to develop precise monitoring method in FSW process.

In FSW process, the physics is not yet fully understood which lead to lack in precise mathematical formulation of the process. Other modeling technique such as finite element modeling is also capable of predicting the strength of the joint. But difficulty arises in the assumptions of the process made during modeling which may not be feasible during the actual welding process. Apart from this, data-driven models can be a more suitable alternate to develop models for the prediction of the weld quality. Lakshminarayanan et al. [20] considered tool rotational speed, welding speed, and plunge force as the process parameters to develop a multi-layer feed-forward neural network trained with back propagation algorithm for the prediction of weld joint strength in FSW process. Prediction of hardness values of the friction stir welded joints had been attempted by Buffa et al. [21] using artificial neural network trained with back propagation algorithm. Shojaeefard et al. [22] also developed neural network models for the prediction of ultimate tensile strength (UTS) and hardness distribution in FSW process. Similar reported works are found in [23–25]. The survey fetched the information that artificial neural network models are one of the most popular methods for data-driven modeling. Advantages with these models are no precise mathematical formulation is required for the process.

The research work presented herewith will explore the application of wavelet packet transformation for efficacious extraction of features from current signatures of main spindle motor and feed motor as this signal processing technique offers more fertility and flexibility. A new method is presented for the selection of the best mother wavelet function by computing the ratio between the energy of the signal and entropy of the decomposed wavelet packet. Principal component analysis is the data reduction method implemented to select the most relevant features among all the features extracted from the signals. Selected signal features along with the process parameters namely tool rotational speed, welding speed, and shoulder diameter are presented to the developed neural network models for the prediction of UTS and yield strength of the joints.

2 Experimental work

AA1100 aluminum alloy plates with dimension 160 × 110 × 6 mm are friction stir welded in butt joint configuration. The two plates are hold tightly together with a specially designed fixture to avoid any mismatch or misalignment during the welding process. In this study, a straight cylindrical tool made of SS316 material is used for the welding process. The shoulder diameter of the tool is varied in four levels with the pin length and diameter fixed at 5.7 and 6 mm,

Table 1 Mechanical properties and chemical composition of AA1100

Mechanical properties	Chemical composition (weight %)
	Al, 99.3
UTS (MPa) = 119.8	Si, 0.2
Yield strength (MPa) = 106	Zn, 0.2
Percentage elongation, 17.1	Fe, 0.2
	Cu, 0.1

respectively. Tensile specimens are prepared as per ASTM E8M standard dimensions and tested in universal testing machine (Make: INSTRON, Model: 8801) at a constant crosshead speed of 1 mm/min. The chemical properties and mechanical properties of base material are listed in Table 1.

A vertical milling machine is adapted to perform FSW process [26]. The main spindle motor is rotated by a 5.5-kW three-phase induction motor. The traversing of the tool is achieved by a three-phase induction feed motor with a rated power of 0.75 kW. Current signals from the main spindle motor and feed motor are acquired using two Hall effect current transducers. All the signals are acquired using a high-speed data acquisition system at a sampling rate of 10 kHz. A schematic representation of the process is shown in Fig. 1.

2.1 Procedure

In FSW process, rotational speed and welding speed are the two most influencing process parameters [1]. Apart from these two, the shoulder diameter of the tool also plays a significant role in heat generation in FSW process which is essential for better plasticization of the material which yields better mixing for good welds [27]. Thus, these three process parameters are considered for investigation. A full factorial design method is implemented to obtain the design matrix to carry out the experiments. All the parameters are varied in four levels. It is obvious that an increase in level increases the number of experimental runs in the power of factor in full factorial design method which increases the experimental cost. A total of 43, i.e., 64, experimental runs are obtained in the design matrix. All the experiments are performed randomly to reduce bias or experimental error. Table 2 listed the experimental runs with measured responses. One experiment (Exp. No. 33) is repeated which is chosen randomly. The objective of repeating an experiment is to test the repeatability of the welding process under the current welding environment. Repeated experiment would bring the effect of uncontrollable parameters during the FSW process in the outcome of the process in terms of UTS (or yield strength) of the joints. UTS of the repeated experiment (Exp. No. 65) reveals a difference of 4.98 MPa than Exp. No. 33 (refer to Table 1). This difference in the UTS is a clear indication of the effect of some uncontrollable parameters other than controllable process parameters (which are the same for both the two experiments Exp. Nos. 33 and 65) on the outcome of the process. This finding is further strengthened by the real-time signals acquired during the welding process as discussed in the later paragraph of this article.

Current signatures from the main spindle motor and feed motor are acquired during the experiments. Sensor scale is set at 10 mV = 1 A for the acquisition of the main spindle motor current signal and 100 mV = 1 A for the acquisition of feed

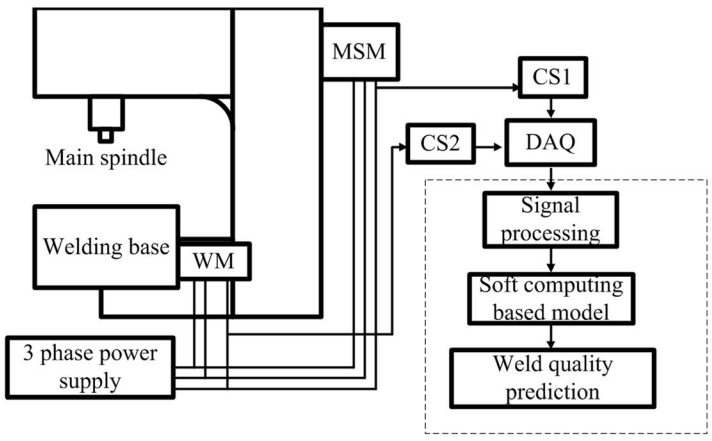

CS1: current sensor for main spindle motor
CS2: current sensor for feed motor
WM: feed motor
MSM: main spindle motor
DAQ: data acquisition system

(a)

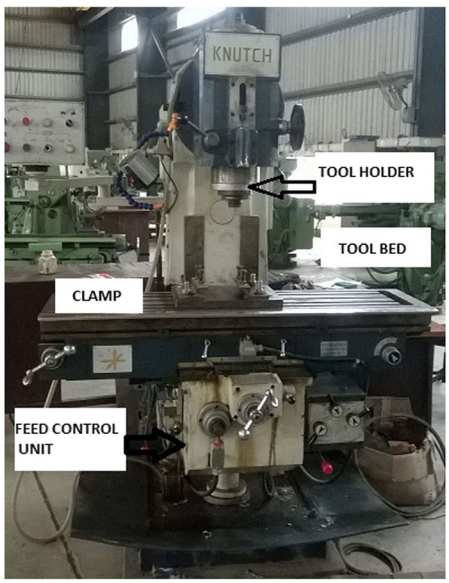

(b)

Fig. 1 **a** Schematic representation of the process. **b** Setup used for the welding experiment

Table 2 Design matrix with responses

Exp. no.	Process parameters			UTS (MPa)	Yield strength (MPa)
	Rotational speed (rev/min)	Welding speed (mm/min)	Shoulder diameter (mm)		
1	600	36	16	94.05	54.32
2	600	36	20	85.87	46.45
3	600	36	24	78.56	43.47
4	600	36	28	65.69	43.10
5	600	63	16	88.42	59.30
6	600	63	20	84.64	43.87
7	600	63	24	88.12	43.85
8	600	63	28	71.88	43.37
9	600	98	16	82.45	63.43
10	600	98	20	85.24	46.04
11	600	98	24	73.60	46.16
12	600	98	28	67.55	40.51
13	600	132	16	95.89	55.58
14	600	132	20	81.89	45.97
15	600	132	24	81.95	44.03
16	600	132	28	84.09	43.23
17	815	36	16	92.00	50.93
18	815	36	20	77.34	48.11
19	815	36	24	85.48	48.18
20	815	36	28	80.33	46.36
21	815	63	16	94.63	53.51
22	815	63	20	78.22	48.56
23	815	63	24	83.13	54.25
24	815	63	28	78.48	42.39
25	815	98	16	73.87	57.23
26	815	98	20	77.90	48.93
27	815	98	24	87.86	42.29
28	815	98	28	65.74	45.24
29	815	132	16	88.05	59.85
30	815	132	20	75.15	49.14
31	815	132	24	92.62	48.19
32	815	132	28	77.83	46.95
33	1100	36	16	74.54	55.11
34	1100	36	20	83.45	44.86
35	1100	36	24	76.30	49.87
36	1100	36	28	51.15	36.79
37	1100	63	16	91.86	51.2
38	1100	63	20	82.69	43.07
39	1100	63	24	89.91	45.98
40	1100	63	28	76.12	43.5
41	1100	98	16	81.41	52.81
42	1100	98	20	77.86	41.27
43	1100	98	24	75.35	45.86
44	1100	98	28	79.28	45.98
45	1100	132	16	95.95	55.35
46	1100	132	20	77.55	48.07
47	1100	132	24	63.91	44.06

Table 2 (continued)

Exp. no.	Process parameters			UTS (MPa)	Yield strength (MPa)
	Rotational speed (rev/min)	Welding speed (mm/min)	Shoulder diameter (mm)		
48	1100	132	28	77.86	41.26
49	1500	36	16	88.42	47.95
50	1500	36	20	64.95	49.77
51	1500	36	24	92.22	54.46
52	1500	36	28	81.08	36.91
53	1500	63	16	92.59	53.72
54	1500	63	20	81.65	41.26
55	1500	63	24	88.92	44.39
56	1500	63	28	68.57	40.63
57	1500	98	16	71.38	60.13
58	1500	98	20	77.17	43.07
59	1500	98	24	87.12	45.37
60	1500	98	28	81.81	38.46
61	1500	132	16	80.29	59.72
62	1500	132	20	83.93	48.09
63	1500	132	24	59.12	43.88
64	1500	132	28	83.64	42.68
65a	1100	36	16	69.56	56.44

[a] Repeated experiment for Exp. No. 33

motor current signal. Magnified view of the current signals from the main spindle motor and feed motor acquired during Exp. No. 33 and Exp. No. 65 is shown in Fig. 2. It is to note that these two experiments are carried out under the same setting of process parameter, although a difference in magnitude of these signals confirms the process variability under the same operating condition. Moreover, UTS and yield strength of the joints from these two experiments also have a considerable difference (refer to Table 2). This provides salient information that any prediction mechanism based only on process parameters may not yield satisfactory results. The change in the signals is a clear indication that signals are carrying some valuable information regarding the process.

2.2 Observations

The variation of UTS and yield strength with the process parameters is investigated keeping two parameters fixed at a time. Figure 3a shows the variation of UTS with rotational speed of the tool. It is observed that with the increase in the rotational speed, UTS values increase up to a certain speed and decrease further. A similar trend in the UTS values is also observed with shoulder diameter (Fig. 3c). But, with the welding speed (shown in Fig. 3b), similar conclusive remarks cannot be drawn. In FSW process, the rotational speed of the tool is mainly responsible for the generation of heat for plasticization of

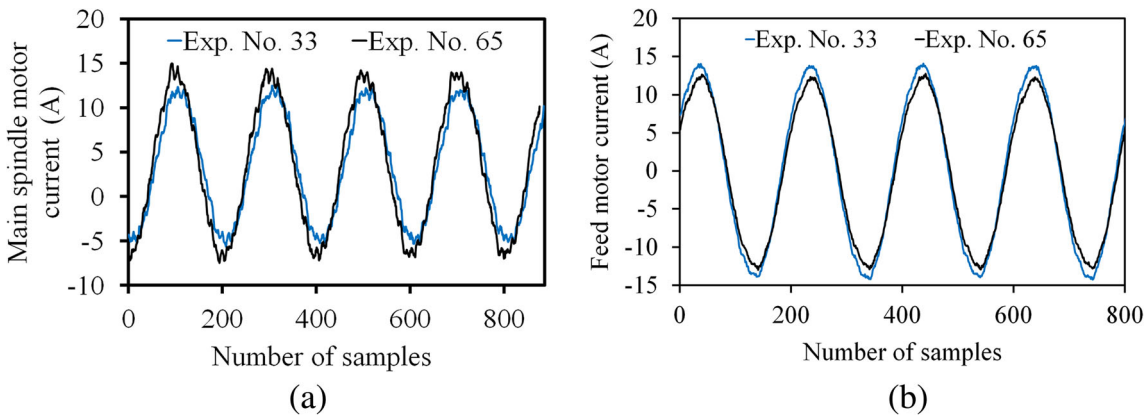

Fig. 2 Magnified view of **a** the main spindle motor current signal **b** feed motor current signal

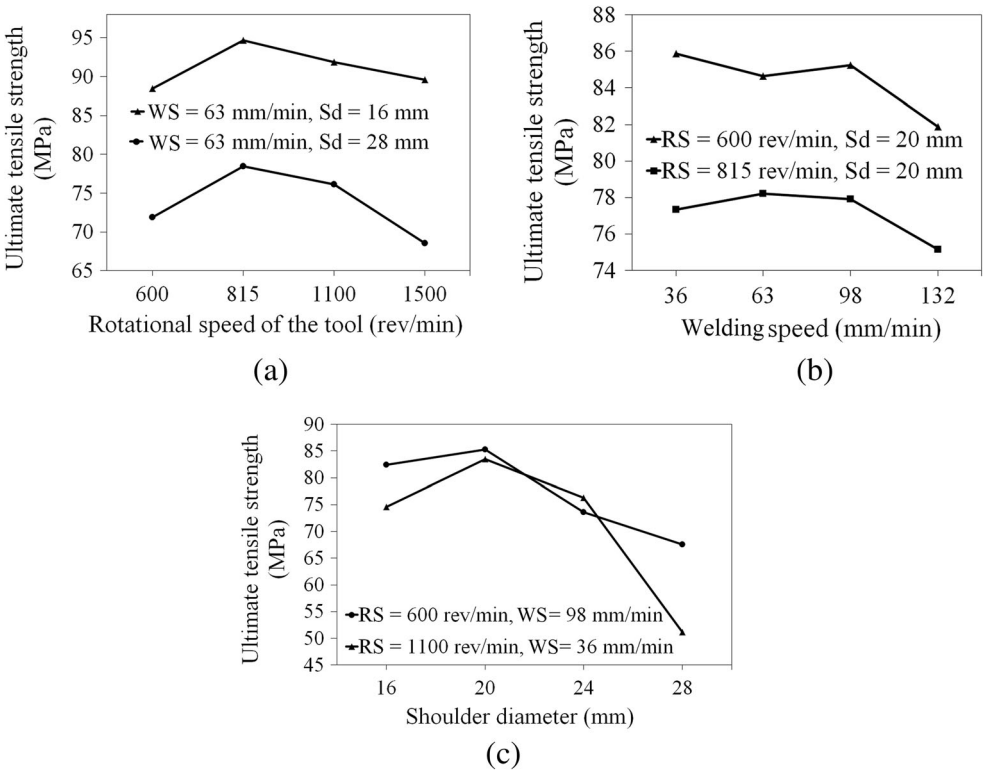

Fig. 3 Variation of UTS with **a** rotational speed, **b** welding speed, and **c** shoulder diameter

the material. Also, the frictional heat generation improves with increase of shoulder diameter. With the increase in these two parameters, heat input to the material increases, resulting in high temperature and high strain rates due to severe mixing of the materials. This may result in grain growth in the material structure which deteriorates the strength of the joints [28]. This is evident from Fig. 3a, c, which demonstrates the case of weld quality deterioration with increase in tool rotational speed and shoulder diameter, respectively. The variation of yield strength with

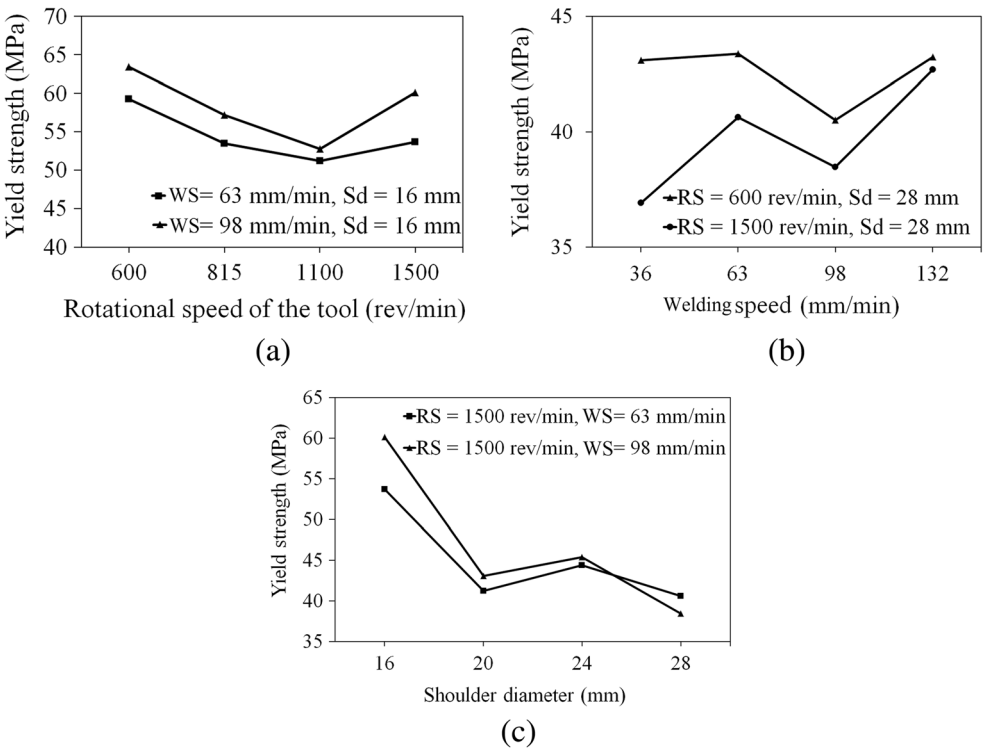

Fig. 4 Variation of yield strength with **a** rotational speed, **b** welding speed, and **c** shoulder diameter

the process parameters is depicted in Fig. 4. Like UTS, the yield strength of the joints does not seem to follow any distinctive trend with the process parameters except with the rotational speed of the tool. Here, with the increase in the rotational speed of the tool, yield strength values follow a decreasing trend up to a certain speed and dramatically increase as the speed increases. Increase in the welding speed of the tool has no effects on the trend and is obvious from Fig. 4b. Similar trends in the variation of these mechanical properties of the joint are also found in literature [29, 30].

3 Wavelet transform as a tool for signal analysis

Fourier transformation (FT) is the most widely used technique for processing of signals. The limitation with FT is that it only retrieves global frequency content of the signal, thus is not suitable for non-stationary signals. On the other hand, wavelet analysis has been proven to be a more flexible and robust method for processing of non-stationary signals due to the characteristics of the wavelet basis function as irregular, asymmetric, and of finite time length [31]. Wavelet transform (WT) of a signal is a function of two parameters namely time and scale, the latter being a key point of the WT. Moreover, WT works with a scaled window, allowing more freedom in the visibility of the entire frequency content, unlike the windowed FT which suffers from limited window size.

Wavelet packet analysis is a generalization of wavelet transformation that offers a richer range of possibilities for signal analysis. In wavelet packet analysis, a signal is split into two parts: approximation and detail. The approximation and detail are both again split into second-level approximation and detail, and the process is repeated to the desired number of level of decomposition. Wavelet packets are particular linear combinations of wavelets. They form the bases that retain the orthogonality, smoothness, and location properties of their parent wavelets [32]. Wavelet packet atoms are waveforms indexed by three naturally interpreted parameters: position, scale, and frequency. In the orthogonal wavelet decomposition procedure, the generic steps split the approximation coefficients into two parts. After splitting a vector of approximation coefficients and a vector of detail coefficients, both at a coarser scale, the information lost between two successive approximations is captured in the detail coefficients. Then, the next step consists of splitting the new approximation coefficient vector; successive details are never reanalyzed. In the corresponding wavelet packet situation, each detail coefficient vector is also decomposed into two parts using the same approach as in approximation vector splitting.

In wavelet packet analysis, a signal $x(t)$ can be represented as the sum of orthogonal wavelet packet function $W_{p,k,l}$ at different scales, oscillations, and localizations.

$$x(t) = \sum_{p} \sum_{k} \sum_{l} C_{p,k,l} W_{p,k,l}(t) \tag{1}$$

where $C_{p,k,l}$ is the wavelet packet coefficients, which can be obtained by the following equation:

$$C_{p,k,l} = \int_{-\infty}^{+\infty} x(t) W_{p,k,l}(t) dt \tag{2}$$

and $W_{p,k,l}$ generated from the base function

$$W_{p,k,l}(t) = 2^{p/2} W_k(2^p t - 1) \tag{3}$$

where indices p, k, and i are the scale, oscillation, and the time localization parameters, respectively ($[(p,l) \in Z^2$ and $k = 0, 1, 2, \ldots \ldots 2^{p-1}]$). In general, wavelet functions are defined by

$$W_{2k}(t) = 2^{1/2} \sum_{l} h_l W_k(2t - l) \tag{4}$$

$$W_{2k+1}(t) = 2^{1/2} \sum_{l} g_l W_k(2t - l) \tag{5}$$

where h_l and g_l are the low pass and high pass filters. $W_0(t) = \phi(t)$ is the scaling function and $W_1(t) = \psi(t)$ is the wavelet function, respectively. The discrete filters h_l and g_l are quadrature mirror filters associated with scaling function and wavelet function, respectively.

Although wavelet transform offers richness in the field of signal processing, it too suffers from few operating limitations. First is the selection of optimal level for decomposition, and second is the selection of proper mother wavelet function for the decomposition of the signals. The published literature shows that mostly, researchers chose the mother wavelet functions either based on previous experience or randomly [33–40]. Therefore, in this study, an attempt has been made to formulate a method for selection of an appropriate mother wavelet function as described in section 3.2.

3.1 Method for finding optimum level of decomposition

In this research, wavelet packet analysis is performed by using MATLAB R2013b built-in functions. A schematic of wavelet packet tree up to the second-level decomposition is shown in Fig. 5 where node W_{00} represents the original signal and W_{20} to W_{23} represent the four

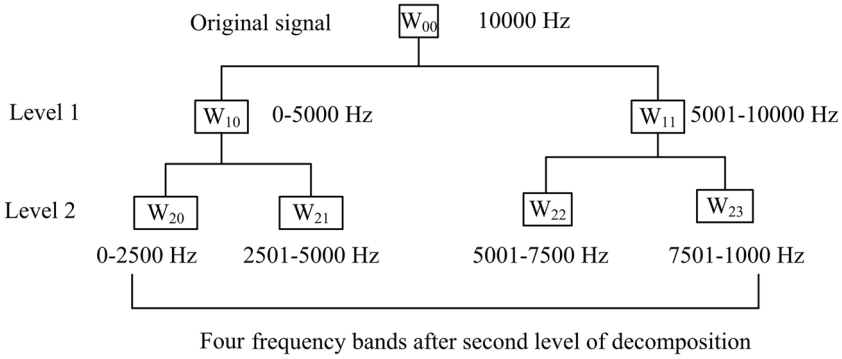

Fig. 5 Wavelet tree after the second level of decomposition

frequency bands obtained after the second level of decomposition. The decomposition can be continued down to the final level where only one element remains in each basis vector. The maximum possible level in case of binary wavelet decomposition is given by

$$j \geq \log_2 N \tag{6}$$

where N is the sampling frequency of the analyzed signal and j is the decomposition level. So, for the present case, $j \geq 14$ since sampling frequency of the signals is 10 kHz. Since this number is very high, the computational time required will be very high to decompose up to this level which is not favorable for any monitoring system.

There are many methods available for the selection of optimum level of decomposition like best on desired frequency band(s), viewing the decomposition signals at different levels, and minimum entropy energy criterion. In this research, minimum entropy energy criterion is used to obtain the best decomposition level. According to entropy criterion, a splitting is only of interest if the entropy of the parent packet is more than the total of the child packets. For computing the entropy values of each packet in the wavelet packet tree, the Shannon entropy method is used. Shannon entropy of a signal S can be computed by the following equation:

$$E(S) = -\sum_{k=1}^{N} S_k{}^2 \log\left(S_k{}^2\right) \tag{7}$$

where $E(S)$ is the Shannon entropy of the signal S and S_k is the k^{th} value of the signal. The entropies of all the packets at different levels are calculated using the abovementioned equation. If the entropy value at node W_{20} is more than the total entropy of nodes W_{30} and W_{31}, then only the splitting would be interesting and decomposition is preceded. Otherwise, not that level can be treated as optimum level of decomposition. In this work, for the main spindle motor current signal, optimum level of decomposition is found to be 6 and that for feed motor current signal is 7.

3.2 Method for finding the best mother wavelet function

In the family of wavelet, there are many wavelet functions available like Haar, Daubechies, Symlet, Coiflet, etc. known as mother wavelet functions. All these functions have different characteristics and to analyze any signal, specific selection of mother wavelet needs to be made for effective extraction of useful features from the signals. However, the selection of mother wavelet functions also affects the extracted features. In this study, a new method is proposed to obtain the suitable mother wavelet. The method proposed is based on a ratio of energy of the signal to the entropy of different wavelet packets as expressed in Eq. (8).

$$\text{Ratio}_i = \left(\frac{E}{En}\right)_i \tag{8}$$

Where i represents the family of the wavelet functions selected for the analysis, E represents the energy of the original signal, and En represents the entropy of the decomposed wavelet packets using the selected mother wavelet functions. For obtaining the entropy of the wavelet packet, the Shannon entropy criterion as expressed in Eq. 7 is chosen in the present study.

Energy of a signal represents the information carried by the signal. Entropy of the decomposed wavelet packets at a particular level of decomposition reflects the amount of disorder in the signal which can be viewed as a measure of uncertainty regarding the information contained in the signal. Hence, wavelet function which fetches lower entropy values at selected level of decomposition should be preferred. The proposed ratio will represent the process information retained by signals as it deals with the original signal information in terms of energy and minimum entropy which reflects the uncertainty in the original signal. For the selection of suitable mother wavelet function, the one with high ratio should be considered. Here, for both the main spindle motor and feed motor current signal, this ratio is calculated using 44 different mother wavelet functions for each signal. The mother wavelet function with the maximum ratio of energy to entropy is

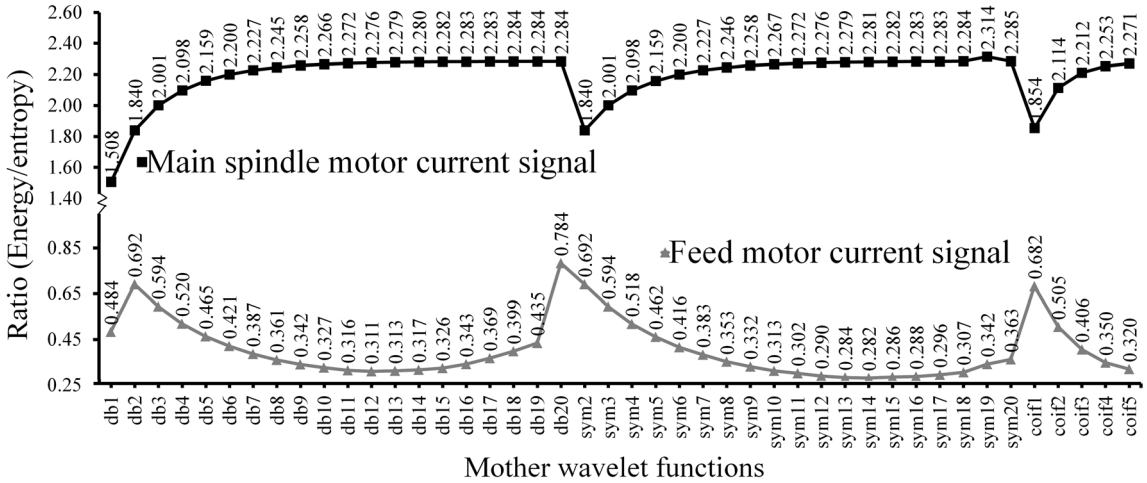

Fig. 6 Variation of computed ratio with mother wavelets for the main spindle motor current signal and feed motor current signal

considered as the best mother wavelet. All the acquired signals against each experiment are tested using the proposed method for finding the appropriate mother wavelet function. Figure 6 represents the ratio of different wavelet functions for the main spindle motor and feed motor current signal against Exp. No. 45 which is the case of maximum UTS value. From the analysis, it is found that symlet19 and db20 are the best mother wavelets for the main spindle motor and feed motor current signals, respectively.

The result obtained using the proposed method is compared with two existing methods namely root mean square difference (RMSD) between the original signal and the reconstructed signal from the wavelet packet tree [32] and correlation coefficient between the wavelet packet coefficients and monitored quantity [31]. The wavelet with the least RMSD and high correlation coefficient among the considered wavelet functions is considered as the best mother wavelet. Figure 7 shows the RMSD of the main spindle motor and feed motor current signal, respectively. Interestingly, this analysis also provides the same result as symlet19 and db20 to be the best mother wavelets for the main spindle and feed motor current signals, respectively. Figure 8 represents the results of the method based on correlation coefficient between the average RMS values of the wavelet coefficients and UTS of the joints.

The two methods selected for the comparison of the results from the proposed method although give the same results but suffer from few limitations. The method based on RMSD [32] of the original and the reconstructed signal is actually performing a noise reduction in the original signal. Once the original signal is decomposed, it is filtered through the wavelet filters. Here, the chances of losing valuable process information are high. It is suggested that the mother wavelet function which gives the least RMSD is suitable for decomposition. But it does not guarantee that the selected mother wavelet function can effectively extract the signal information which contains the valuable information of process variations. The selected mother wavelet can be a better candidate for noise elimination from the original signal.

The other method used for the comparison suggests finding a correlation coefficient [31] between the average root mean square values of the wavelet packets with the parameter that is monitored using the signal information. Here, the value of the parameter monitored depends on the accuracy of the measurement procedure adapted. This is not suitable for approaches which concentration is to extract information contained in a signal. The selection from this approach depends on the accuracy of measurement of the parameter being monitored and can be hindered due to many external factors. Hence, selection of mother wavelet based on this approach may contain redundancy in the information extracted from signal. On the other hand, the proposed method based on the ration of the energy of the original signal to the entropy of the decomposed wavelet packet does not suffer from the abovementioned limitations. It purely depends on signal information which can detect characteristics of the process being monitored with signals. Thus, the proposed method can be a suitable alternate approach for the selection of mother wavelet function for effective decomposition of signals.

Mother wavelet function in wavelet analysis bears different characteristics which will affect the decomposition process. Thus, it is essential to precisely select the wavelet function in order to obtain a suitable decomposition. The decomposed wavelet packets at a particular level of decomposition carry the information retained by original signal. Hence, first, the optimum level needs to be selected. In this study, the Shannon entropy criterion is used for this purpose. Once the optimum level is found, each signal is decomposed to the optimum level of decomposition with different mother wavelet functions and the ratio against each signal is computed using Eq. 8. This is repeated for each acquired signal and an array consisting of ratios for each signal is obtained for each mother wavelet function. From this array, the mother wavelet function which

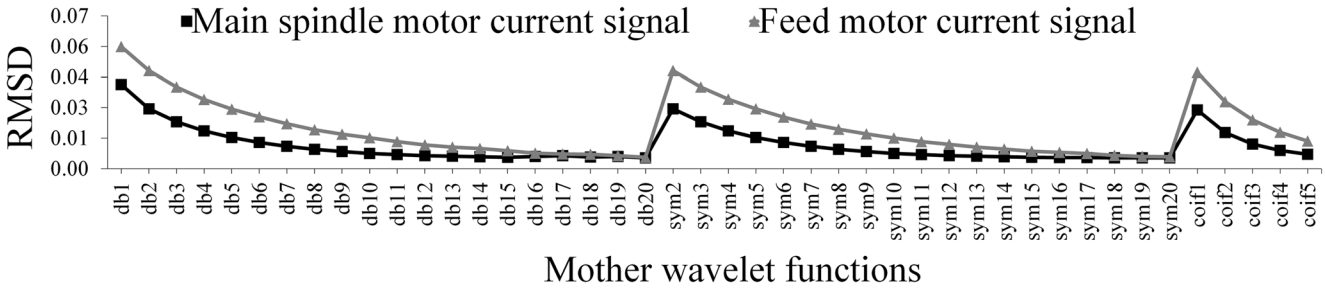

Fig. 7 Variation of computed root mean square difference values with mother wavelet functions for the main spindle motor current signal and feed motor current signal

yield maximum ratio is considered as the best mother wavelet. Then, the signals are decomposed to the optimum level using the best mother wavelet function. For the present study, Symlet 19 and Daubechies 20 are the best mother wavelet functions obtained for the main spindle motor current signal and feed motor current signal respectively.

4 Effective selection of signal features

Wavelet packet coefficients are extracted using the wavelet packet analysis for each signal and a list is obtained containing the signal features. From the wavelet packet analysis, a total of 192 (64 for the main spindle motor current and 128 for feed motor current) features are obtained. But it is very difficult to handle such a large number of features and it is not essential too, that all these features would be equally effective for modeling the weld quality. Moreover, multiple features may contain same information. To extract the most appropriate features for both the signals, data reduction method is essential. In this research, principal component analysis (PCA) is chosen as data reduction technique and to find out most eligible features from the available 192 features.

Principal component analysis (PCA) is mathematically defined [41] as an orthogonal linear transformation that transforms a number of (possibly) correlated variables into a (smaller) number of uncorrelated variables called principal components. The first principal component accounts for the greatest statistical variability and second greatest variance represented by the second component respectively and so on. PCA is theoretically the representation of the optimum transform for the given data in least square terms. The idea of PCA lies in calculating the eigenvectors and eigenvalues of the covariance matrix of the data and is efficiently calculated by singular value decomposition. These eigenvectors describe an orthonormal basis that is effectively a rotation of the original Cartesian basis. Each principal component is a linear combination of the original variables. All the principal components are orthogonal to each other, so there is no redundant information. The principal components as a whole form an orthogonal basis for the space of the data [42].

The percentage variability explained by the first ten components for the main spindle motor and feed motor current signals are shown in Fig. 9. It is observed that, in case of main spindle motor current signal features, first five components account for the 99.87 % variability of the entire data set whereas the percentage variability of the rest of the dataset is only 0.13 %. So, first five components are chosen as the features for the case of main spindle motor current signal. In case of feed motor current signal, out of first 14 components, first four components represent 99.81 % of total variability leaving the rest for the other components. Thus, first four components are judged to be effective feature space to represent the information contained in the feed motor current signal and are

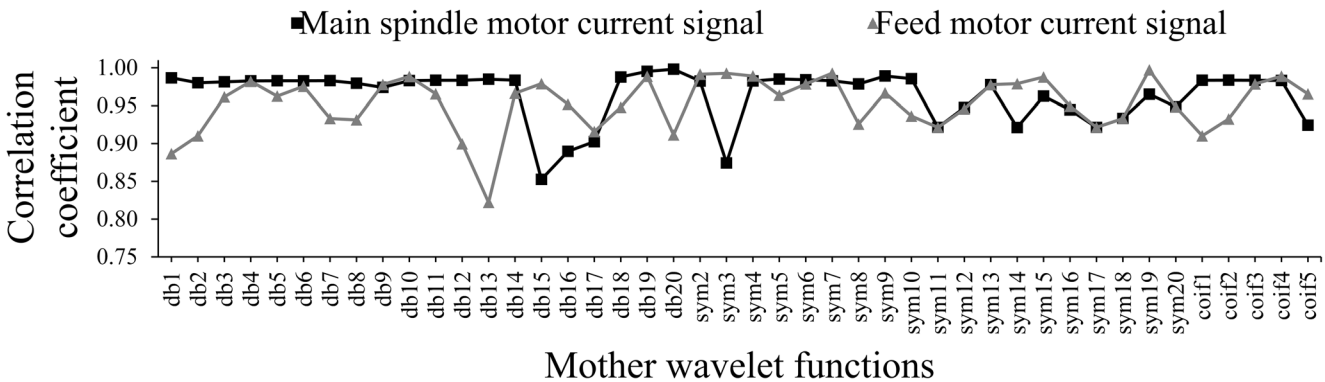

Fig. 8 Variation of correlation coefficient with mother wavelet functions for the main spindle motor current signal and feed motor current signal

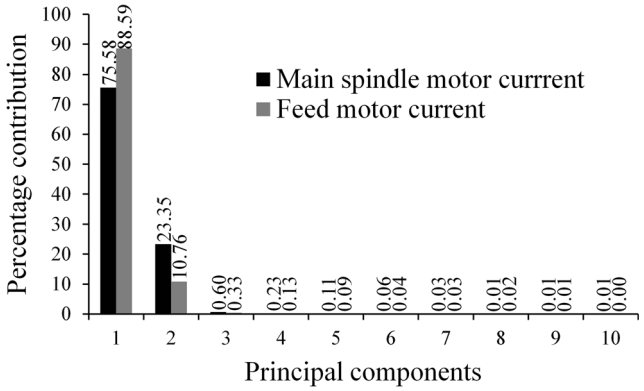

Fig. 9 Percentage contribution of principle components for wavelet packet features of the main spindle motor and feed motor current signals

treated as the features for further analysis. Thus, a total of nine signal features are extracted from the main spindle motor and feed motor current signals for further analysis.

5 Artificial neural network model

The details of the ANN modeling are well documented in the literature and interested reader can refer to the technical article [41]. In the presented research work, two types of neural networks are developed for modeling of UTS and yield strength of the welds. One is the standard multi-layer neural network (MLNN) with back propagation training algorithm, commonly known as back propagation neural network (BPNN) and the other one is radial basis function neural network. In this work, out of 65 data sets, 48 are used as training, 10 are used as validation, and remaining 7 are used as the testing data sets. The data sets are chosen randomly. The input space of the developed models contain 12 inputs among which three are process parameters and rest nine are the extracted signal features.

5.1 Weld quality modeling using back propagation neural network

Two BPNN models are developed for the prediction of UTS and yield strength of the welded joints. The developed BPNN models in this study contain single hidden layer, in which the number of hidden neurons are varied in between 5 to 39 in steps of 1. Learning rate (η) and momentum coefficient (α) for weight updation are varied in between 0.1 to 1 and 0.01 to 1 in steps of 0.04, respectively. Initial weight values are chosen randomly between ±0.9 and the bias values at the output layer is taken as 0 and that for input and hidden layers as 1.0. All the inputs and output variables are normalized between 0.1 and 0.9 which ensures that the back propagation algorithm does not drive some of the connection weights to infinity and thus slow down the training [42]. The activation functions for both the hidden and output layer neurons are log-sigmoid. The optimum number of hidden neuron is selected based on the minimum of the sum of training and validation MSE.

The variation of MSE with the number of hidden neurons in case of BPNN model for the UTS is shown in Fig. 10a. It can be seen that against hidden neuron number 19 minimum MSE is observed. Thus, 19 numbers of hidden neurons are considered as the optimal number for modeling of UTS. With this optimum number of hidden neurons, optimum learning rate and momentum coefficients are obtained. The variation of

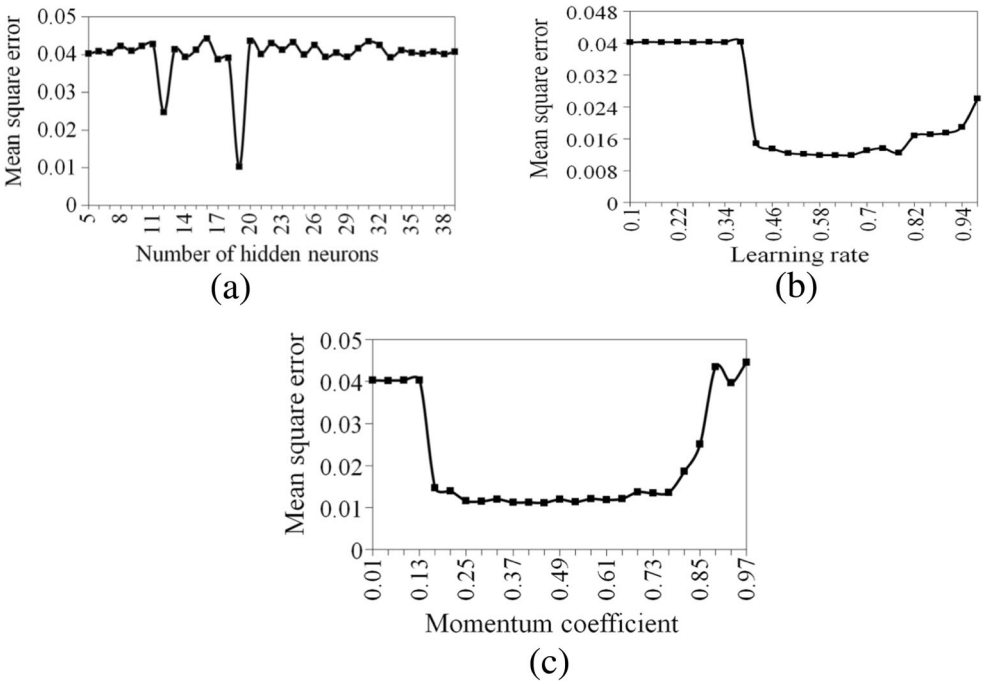

Fig. 10 Variation of MSE of BPNN model for UTS with **a** number of hidden neurons, **b** learning rate, and **c** momentum coefficient

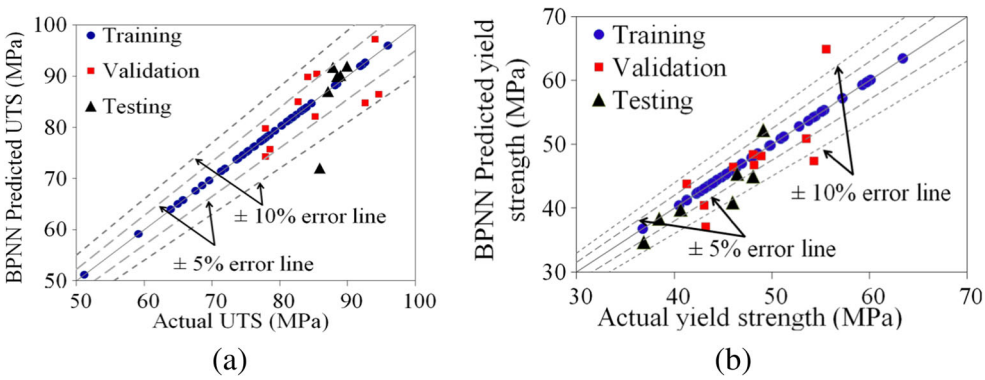

Fig. 11 Scatter diagram for BPNN model for **a** UTS prediction and **b** yield strength prediction

MSE with learning rate and momentum coefficient is shown in Fig. 10b, c, respectively. From these two figures, optimum learning rate and momentum coefficient are found out to be 0.62 and 0.53, respectively. Thus, the optimum network structure of the developed BPNN model for UTS comes out to be 12-19-1 with $\eta = 0.62$ and $\alpha = 0.53$. Similar procedure has been applied to find the optimum network structure and parameters for yield strength prediction. Optimum BPNN model for yield strength is found to be 12-21-1 with $\eta = 0.62$ and $\alpha = 0.61$. The comparison of predicted UTS and yield strength with actual UTS and yield strength is shown as scatter plot in Fig. 11a–b, respectively. Prediction statistics for UTS and yield strength is tabulated in Tables 3 and 4, respectively. Absolute average percentage error for the testing cases for UTS and yield strength are 5.87 and 4.93, respectively. These results (Fig. 11 and Tables 3 and 4) indicate that BPNN model can be effectively used for prediction of UTS and yield strength.

5.2 Weld quality modeling using radial basis function neural network

To compare the prediction performance of BPNN model, one more neural network model is developed known as radial basis function neural network (RBFNN). In the current study, the Gaussian function is used as radial basis function and the activation function for the output neurons are chosen as sigmoid function. Initial centers and spread of the Gaussian function are chosen randomly and updated through supervised learning scheme. The details of supervise learning algorithm for RBFNN can be found elsewhere [43]. In finding the optimal network parameters for this model, different combinations of number of hidden neurons, learning rate for weight updation, center updation, and the Gaussian function spread updation are tried and based on the minimum of sum of training and validation, MSE criterion optimum parameters are obtained. Two different RBFNN models are developed like in BPNN, for modeling of UTS and yield strength. Numbers of hidden neurons are varied in between 5 to 40 in steps of 1. Learning rate for updating weights is varied in between 0.1 to 1 in steps of 0.04. Learning rate for center and spread updation is varied in between 0.01 to 1 in steps of 0.4.

The variation of MSE with number of hidden neurons, learning rate for weight, and center and spread updation is shown in Fig. 12a–d for the modeling of UTS. Based on the minimum MSE criterion, optimum number of hidden neurons for UTS prediction is found to be 15 and for yield strength prediction 18, respectively. The optimal network

Table 3 Comparison between BPNN and RBFNN predicted outputs for testing cases for UTS

Exp. no.	Actual UTS (MPa)	BPNN model		RBFNN model	
		Predicted UTS (MPa)	% error	Predicted UTS (MPa)	% error
39	89.91	91.94	−2.25	74.76	16.84
59	87.12	86.99	0.14	61.77	29.09
2	85.87	71.99	16.16	75.71	11.83
29	88.05	101.51	−15.28	77.15	12.37
27	87.86	91.67	−4.33	78.95	10.13
55	88.92	90.13	−1.32	57.55	35.27
49	88.42	89.87	−1.64	72.45	18.05
Absolute average percentage error			5.87		19.08

Table 4 Comparison between BPNN and RBFNN predicted outputs for testing cases for yield strength

Exp. no.	Actual yield strength (MPa)	BPNN model		RBFNN model	
		Predicted yield strength (MPa)	% error	Predicted yield strength (MPa)	% error
39	45.98	40.93	10.97	41.81	9.06
56	40.63	39.80	2.02	37.91	6.69
2	46.45	45.40	2.24	43.19	7.01
30	49.14	52.25	−6.34	48.88	0.52
18	48.11	44.96	6.53	42.24	12.18
60	38.46	38.32	0.35	39.18	−1.88
52	36.91	34.66	6.07	38.06	−3.12
Absolute average percentage error			4.93		5.78

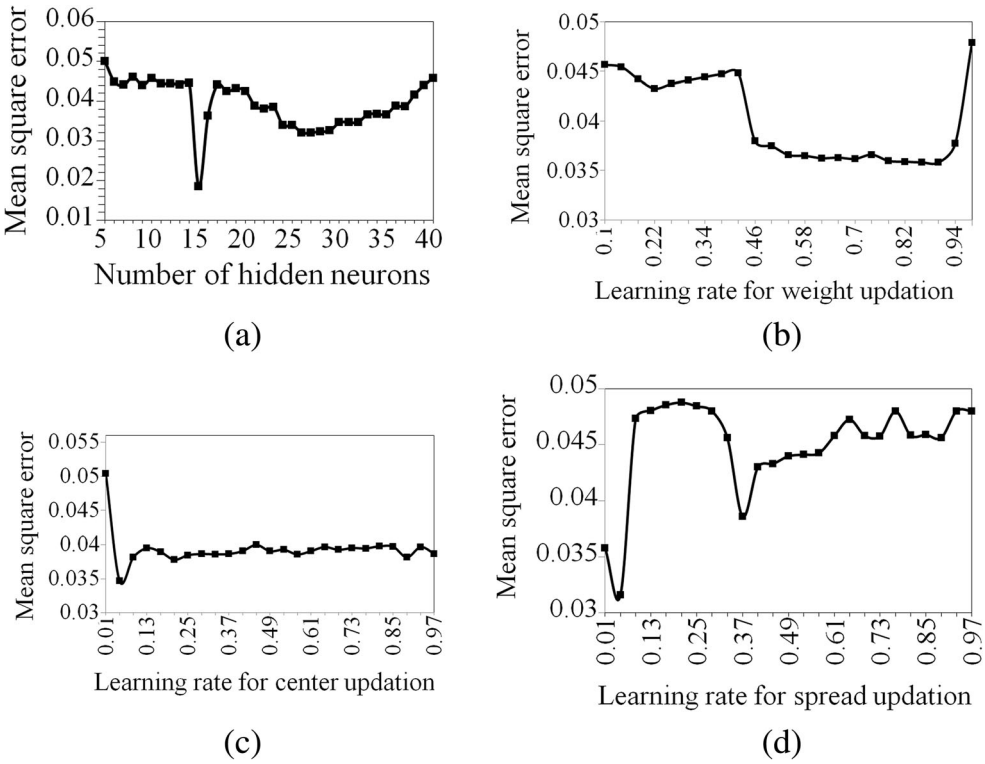

Fig. 12 Variation of MSE for RBFNN model for UTS with **a** number of hidden neurons, **b** learning rate for weight updation, **c** learning rate for center updation, and **d** learning rate for spread updation

structure for UTS modeling is found to be 12-15-1 with 0.9, 0.05 and 0.05 to be the optimum learning rates for weight and center and spread updation, respectively. For the prediction of yield strength, 12-18-1 with 0.9, 0.05, and 0.05 are found to be the optimum learning rates for weight and center and spread updation, respectively. Scatter plots for the comparison of predicted versus actual values of UTS and yield strength are shown in Fig. 13a–b. It is observed from the figures that RBFNN prediction of UTS is inferior as compared to yield strength prediction. Average absolute prediction error for the testing cases for UTS and yield strength are 19.08 and 5.78 %, respectively. It can be seen that RBFNN prediction is also better for yield strength than UTS of the joints. However, the prediction performance of RBFNN model is inferior to that of BPNN model for both the UTS and yield strength.

The research output of the proposed work demonstrates an avenue to implement real-time monitoring of weld quality in FSW process. Once the model is trained and tested, the same can be used to predict weld quality for any unknown condition and process variation by feeding process parameter and motors signals. The proposed technique is simple but reasonably accurate, and it can be implemented without changing the existing setup. This approach can be a better alternative to the existing methods currently being practiced for the qualitative assessment of welded joints.

6 Conclusions

Application of wavelet packet analysis for efficacious extraction of features from current signals from main spindle and

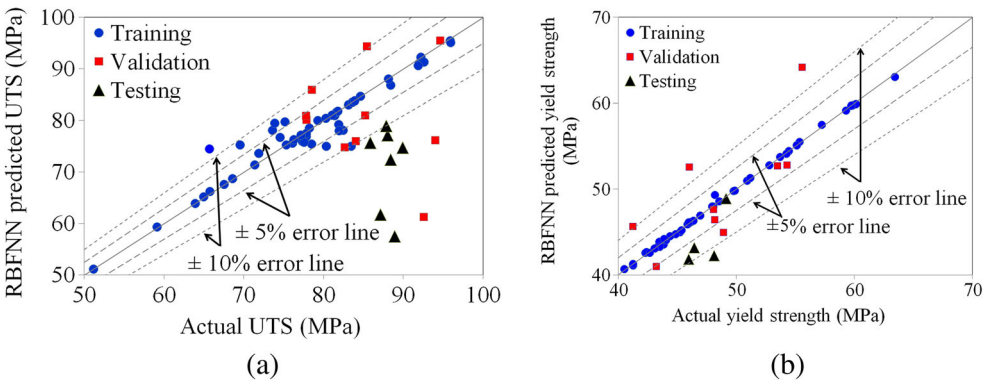

Fig. 13 Scatter diagram for RBFNN model for **a** UTS prediction and **b** yield strength prediction

feed motor are presented. A new method for selecting the best mother wavelet is presented and compared with two existing methods. This new method computes the ratio between the energy and entropy of the signal. The results of the proposed method are found to be in exact agreement with the results of the existing method. The mother wavelet function corresponding to the maximum ratio value is chosen to be the best among 44 different wavelet functions considered in this study. For the selection of suitable level of decomposition, the Shannon entropy criterion is used. For the main spindle motor current analysis, symlet19 is found to be the suitable mother wavelet function with an optimum level of decomposition of 6. Whereas, for feed motor current, db20 is the suitable mother wavelet function with 7 being the optimum level of decomposition. Using wavelet packet analysis, a total of 192 features are computed and it is reduced to 9 most effective features using principle component analysis. The selected relevant features along with tool rotational speed, welding speed, and shoulder diameter are fed to two developed neural network models: multi-layer feed-forward neural network trained with back propagation algorithm and radial basis function neural network for the prediction of ultimate tensile strength and yield strength. Both the developed models achieve a better prediction in case of yield strength than modeling of ultimate tensile strength of the joints. However, among these two models, accuracy of BPNN model is found to be better than RBFNN for prediction of both ultimate tensile strength and yield strength.

Acknowledgments The authors gratefully acknowledge the financial support provided by SERB (Science & Engineering Research Board), INDIA (grant no. SERB/F/2767/2012-13) to carry out this research work.

References

1. Mishra RS, Ma ZY (2005) Friction stir welding and processing. Mater Sci Eng R 50:1–78
2. Boldsaikhan E, Corwin EM, Logar AM, Arbegast WJ (2011) The use of neural network and discrete Fourier transform for real-time evaluation of friction stir welding. Appl Soft Comput 11:4846–4893
3. Trummera VR, Suzano E, Beltrão M, Roos A, Santos JF, Castro PMST (2012) Influence of the FSW clamping force on the final distortion and residual stress field. Mater Sci Eng A 538:81–88
4. Yang Y, Kalya P, Landers RG, Krishnamurthy K (2008) Automatic gap detection in friction stir butt welding operations. Int J Mach Tools Manuf 48:1161–1169
5. Fleming PA, Lammlein DH, Wilkes DM, Fleming KA, Bloodworth TS, Cook GE, Strauss A, DeLapp D, Lienert T, Bement M, Prater T (2008) In-process gap detection in friction stir welding. Sens Rev 28(1):62–67
6. Cavaliere P, Campanile G, Panella F, Sqillace A (2006) Effect of welding parameters on mechanical and microstructural properties of AA6065 joints produced by friction stir welding. J Mater Process Technol 180:263–270
7. Trimble D, Monaghan J, Donnell GE (2012) Force generation during friction stir welding of AA2024-T3. CIRP Ann Manuf Technol 61:9–12
8. Das B, Pal S, Bag S (2016) A combined wavelet packet and Hilbert-Huang transform for defect detection and modelling of weld strength in friction stir welding process. J Manuf Process 22:260–268
9. Subramaniam S, Narayan S, Denis AS (2013) Acoustic emission-based monitoring approach for friction stir welding of aluminum alloy AA6063-T6 with different tool pin profiles. Proc IMechE Part B J Eng Manuf 227(3):407–416
10. Chen C, Kovacevic R, Jandgric D (2003) Wavelet transform analysis of acoustic emission in monitoring friction stir welding of 6061 aluminum. Int J Mach Tools Manuf 43:1383–1390
11. Zeng WM, HL W, Zhang J (2006) Effects of tool wear on microstructure, mechanical properties and acoustic emission of friction stir welding of 6061 aluminium alloy. ACTA Metall Sin (Engl Lett) 19:9–19
12. Pal S, Pal SK, Samantaray AK (2010) Prediction of the quality of pulsed metal inert gas welding using statistical parameters of arc signals in artificial neural network. Int J Comput Integr Manuf 23(5):453–465
13. Sick B (2002) On-line and indirect tool wear monitoring in turning with artificial neural networks: a review of more than a decade of research. Mech Syst Signal Process 16(4):487–546
14. Liu TI, Kumagai A, Wnag YC, Song SD, Fu Z, Lee J (2010) On-line monitoring of boring tools for control of boring operations. Robot Comput Integr Manuf 26:230–239
15. He K, Li X (2014) A quantitative estimation technique for welding quality using local mean decomposition and support vector machine. J Int Manag. doi:10.1007/s10845-014-0885-8.
16. Hunag PL, Li JF, Sun J, Jia XM (2016) Cutting signals analysis in milling titanium alloy thin-part components and non-thin wall components. Int. J. Adv. Manuf. Technol. (84):2461–2469.
17. He K, Li Q, Chen J (2013) An arc stability evaluation approach for SW AC SAW based on Lyapunov exponent of welding current. Measurement 46(1):272–278
18. He K, Zhang Z, Xiao S, Li X (2013) Feature extraction of AC square wave SAW arc characteristics using improved Hilbert-Huang transform and energy entropy. Measurement 46(4):1385–1392
19. Das B, Pal S, Bag S (2014) Monitoring of friction stir welding process through signals acquired during the welding. 5th International & 26th All India Manufacturing Technology, Design and Research Conference (AIMTDR 2014) December 12th–14th, 2014, IIT Guwahati, Assam, India.
20. Lakshminarayanan AK, Balasubramanian V (2009) Comparison of RSM with ANN in predicting tensile strength of friction stir welded AA7039 aluminium alloy joints. Trans Nonferrous Metals Soc China 19:9–18
21. Buffa G, Fratini L, Micari F (2012) Mechanical and microstructural properties prediction by artificial neural networks in FSW processes of dual phase titanium alloys. J Manuf Process 14:289–296
22. Shojaeefard MH, Behnagh RA, Akbari M, Givi MKB, Farhani F (2013) Modeling and Pareto optimization of mechanical properties of friction stir welded AA7075/AA5083 butt joints using neural network and particle swarm algorithm. Mater Des 44:190–198
23. Tansel IN, Demetgul M, Okuyucu H, Yapici A (2010) Optimizations of friction stir welding of aluminum alloy by using genetically optimized neural network. Int J Adv Manuf Technol 48: 95–101
24. Dhanunjaya Y, Reddy A, Pratihar DK (2011) Neural network-based expert systems for predictions of temperature distributions in electron beam welding process. Int J Adv Manuf Technol 55:535–548
25. Roshan SB, Jooibari MB, Teimouri R, Ahmadi GA, Naghibi MF, Sohrabpoor H (2013) Optimization of friction stir welding process

of AA7075 aluminum alloy to achieve desirable mechanical properties using ANFIS models and simulated annealing algorithm. Int J Adv Manuf Technol 69:1803–1818
26. Minton T, Mynors DJ (2006) Utilisation of engineering workshop equipment for friction stir welding. J Mater Process Technol 177(1–3):336–339
27. Arora KS, Pandey S, Schaper M, Kumar R (2010) Effect of process parameters on friction stir welding of aluminum alloy 2219-T87. Int J Adv Manuf Technol 50:941–952
28. Moataz MA, Salem HG (2005) Friction stir welding parameters: a tool for controlling abnormal grain growth during subsequent heat treatment. Mater Sci Eng A 391:51–59
29. Mao Y, Ke L, Liu F, Huang C, Chen Y, Liu Q (2015) Effect of welding parameters on microstructure and mechanical properties of friction stir welded joints of 2060 aluminum lithium alloy. Int J Adv Manuf Technol. doi:10.1007/s00170-015-7191-2
30. Sakthivel T, Sengar GS, Mukhopadhyay J (2009) Effect of welding speed on microstructure and mechanical properties of friction-stir-welded aluminum. Int J Adv Manuf Technol 43:468–473
31. Pal S, Heyns PS, Freyer BH, Theron NJ, Pal SK (2011) Tool wear monitoring and selection of optimum cutting conditions with progressive tool wear effect and input uncertainties. J Intell Manuf 22(4):491–504
32. Ngui WK, Leong MS, Hee LM, Abdelrhman AM (2013) Wavelet analysis: mother wavelet selection methods. Appl Mech Mater 393:953–958
33. Li X (1998) Real-time detection of breakage of small diameter drills with wavelet transform. Int J Adv Manuf Technol 14:539–543
34. Kwak JS (2006) Application of wavelet transform technique to detect tool failure in turning operations. Int J Adv Manuf Technol 28:1078–1083
35. Hua W, Guanlong C, Ping Z, Zhongqin L (2006) Periodic trend detection from CMM data based on the continuous wavelet transform. Int J Adv Manuf Technol 27:733–737
36. Ao Y, Qiao G (2010) Prognostics for drilling process with wavelet packet decomposition. Int J Adv Manuf Technol 50:47–52
37. Kwak JS, Ha MK (2004) Detection of dressing time using the grinding force signal based on the discrete wavelet decomposition. Int J Adv Manuf Technol 23:87–92
38. Yu G, Li C, Kamarthi S (2009) Machine fault diagnosis using cluster-based wavelet feature extraction and probabilistic neural network. Int J Adv Manuf Technol 42:145–151
39. Chen X, Li B (2007) Acoustic emission method for tool condition monitoring based on wavelet analysis. Int J Adv Manuf Technol 33:968–976
40. Abu-Zahra NH, Lange JH (2002) Tool chatter monitoring in turning operations using wavelet analysis of ultrasound waves. Int J Adv Manuf Technol 20:248–254
41. Humberstone M, Wood B, Henkel J, Hines JW (2012) Differentiating between expanded and fault conditions using principal component analysis. J Intell Manuf 23:179–188
42. Haykin S (2003) Neural networks: a comprehensive foundation. Pearson Education, Delhi
43. Taghi M, Baghmisheh V, Pavesic N (2004) Training RBF networks with selective backpropagation. Neurocomputing 62:39–64